Am J Cancer Res 2022;12(2):537-548
www.ajcr.us /ISSN:2156-6976/ajcr0140507

Original Article

AHRR contributes to inflammatory lymphangiogenesis by activating the EPAS1/VEGFD signaling axis in head and neck cancer

An Hu[1*], Jian-Wei Zhang[1*], Li-Yun Yang[1*], Pei-Pei Qiao[1,2*], Dan Lu[1]

[1]Department of Otolaryngology-Head and Neck Surgery, Gongli Hospital, Second Military Medical University, Pudong New Area, Shanghai 200135, China; [2]The Graduate School, Ningxia Medical University, Yinchuan 750004, Ningxia, China. [*]Equal contributors.

Received November 12, 2021; Accepted January 20, 2022; Epub February 15, 2022; Published February 28, 2022

Abstract: Lymph node metastasis (LNM) is associated with poor survival in patients with Head and Neck cancer (HNC). Aryl hydrocarbon receptor repressor (AHRR) is thought to be responsible for increased lymphangiogenesis and LNM. AHRR and endothelial PAS domain-containing protein 1 (EPAS1) are basic helix-loop-helix/per-arnt-sim family transcription factors, however, its central role in lymphangiogenesis remains to be explored. In this study, we explored that EPAS1 dimerizes with HIF-1β during lymphangiogenes and tumor growth, inducing expression of many genes, including vascular endothelial growth factor-d (VEGFD). AHRR wild-type (*Ahrr*$^{+/+}$) transgenic carcinoma of the mice develop tumors with greater frequency than AHRR-null (*Ahrr*$^{-/-}$) mice, even though prevalence of squamous epithelial hyperplasia is not inhibited. Hypoxia induced VEGFD protein in a genotype-dependent fashion in *Ahrr*$^{+/+}$, *Ahrr*$^{+/-}$ and *Ahrr*$^{-/-}$ HNC. However, hypoxia induced upstream proteins in the phosphatidylinositol 3-kinase-signaling cascade to a similar extent in HNC of each *Ahrr* genotype, evidenced by Akt phosphorylation. These findings suggest that AHRR induces HIF-1β expression, increasing interaction with EPAS1 enhancing VEGFD production and lymphangiogenesis in HNC.

Keywords: AHRR, head and neck cancer, EPAS1, HIF-1β, lymphangiogenesis

Introduction

The head and neck cancer (HNC) belong to an invasive malignant tumor with low 5-year survival rate and terribly poor prognosis [1]. Only a small number of patients can undergo effective surgical excision while most patients suffer from metastatic diseases [2]. A major reason for the low survival rate is the distant lymph node and occult cervical metastases [3]. Therefore, suppression of lymph node metastases is essential to improve the survival rate of HNC patients and prevent subsequent metastasis to distant visceral organs [4].

Nevertheless, lymphangiogenesis is closely related to the development and occurrence of lymph node metastases (LNM) [5]. The results showed that vascular endothelial growth factor-d (VEGFD) was the main regulator of lymphangiogenesis [6]. The activation of VEGFD signaling pathway can increase lymphatic vessel density and promote lymphangiogenesis and lymphatic endothelial cell proliferation, and promote the lymphatic node proliferation of tumors [7]. Recent findings discovered that VEGFD pathway is associated with lymph node metastasis, recurrence and prognosis in HNC patients [8]. However, the molecular mechanism of increased expression of VEGFD in tumors promoting lymph node metastasis or lymphangiogenesis remains to be elucidated [9].

Aryl hydrocarbon receptor repressor (AHRR) is important regulator of gene expression that needs to be dimerized with HIF-1β, many of them are important components of cell and exogenous metabolism [10, 11]. Hypoxia-inducible factors (HIFs) are key factors regulating the adaptive response to hypoxia [12-14]. Both the AHRR and EPAS1 are members of the

class I bHLH/PAS protein family. The bHLH proteins regulate the expression of various genes, and heterodimers must be formed with other bHLH proteins to perform their multiple functions [15]. Many studies have assessed the interactions between AHRR signaling and hypoxic environment [16, 17]. Although AHRR have non-classical mechanisms, which leads to interference and crosstalk with other signaling pathways and transcription factors, this study will focus on the signal interference between exogenous response pathways and low oxygen environments, and elucidate its potential mechanism.

Methods

Patient and tumor samples

Paraffin embedded tumor specimen from 161 patients with squamous cell carcinoma of the head and neck were included in this research [18]. We excluded patients who had received preoperative radiotherapy or neoadjuvant chemotherapy, as well as patients with distant metastasis, carcinoma in situ and history of other malignancies at the time of diagnosis. This research program was approved by the Institutional Review Committee of medicine school of Shanghai Jiaotong University.

Cell culture

The human HNCs (FaDu cells and Cal27 cells) were purchased from the ATCC, (USA, VA, Manassas) and cultured in Dulbecco Modified Eagle Medium supplemented with 100 lg/ml kanamycin and 10% fetal bovine serum at 37°C under a 5% CO_2 atmosphere [19]. According to the manufacturer's instructions, 5×10^4 cells per hole were inoculated on fibronectin coated 24-well plate, and proliferation tests were performed. Assessment of each case in triplicate.

Generation and characterization of $Ahrr^{+/+}$, $Ahrr^{+/-}$ and $Ahrr^{-/-}$ FaDu cells

All transfections were performed by electroporation using 1 millifarad capacitor array charged at 350 V. P1 clone containing mouse Ahrr gene was obtained from Genomic System. The target structure was generated by inserting the 2.7-kb KpnI fragment containing the 5' end of the bHLH exon of the Ahrr gene into the KpnI site of pPNT, and then connecting the 5.2-kb KpnI/NotI fragment containing the 3' end of the same bHLH domain. The resulting structure was linearized and electroporated into R1 FaDu cells by NotI digestion. Homologous recombinants selected by Gancyclovir (1 mM) and G418 (0.25 mg/ml) were screened by Southern hybridization. In addition to the endogenous 6-kb fragment, the 300-bp BamHI/XbaI fragment from the Ahrr gene was used to detect the presence of recombinant 8-kb EcoRI band. Heterozygous clones were sub-cultured onto gelatin-coated plates and 3 mg/ml G418 selection was performed to obtain $Ahrr^{+/-}$ and $Ahrr^{-/-}$ cells. Proteins were extracted from these clones, separated by SDS-PAGE, transferred to nitrocellulose, and detected with polyclonal antibodies against the C-terminus of the AHRR protein.

Cell colony formation and viability test

Cells were inoculated in 96-well plate at the rate of 2,000 cells per hole and cultured with 5% CO_2 in a 37°C incubator. CCK-8 tests were measured for Human Lymphatic Endothelial Cells (HLECs) as described above at 0, 12 and 24 h. Assessment of each case in triplicate.

Animal experiments

Animals were obtained from the National Cancer Institute and maintained by the Animal Resource Facility of Medical College of Shanghai Jiaotong University [19]. Animal experiments and care was carried out strictly follow the "guidelines for the use and care of experimental animals" and "principles for the care and use of vertebrates", and was approved by the experimental animal ethic board of the Medical College of Shanghai Jiaotong University. Mice were exposed to 92% N_2/8% O_2 under one atmospheric pressure in a closed plastic room, which was ventilated and humidified to minimize the change of pCO_2. At the end of the experiments, nude mice were killed with excessive sodium pentobarbital (4%, 200 mg/kg via intraperitoneal injection; Sigma, Shanghai, China).

Tumor xenotransplantation model

As mentioned earlier, the HNC xenotransplantation model was established in mice, and the associates were euthanized four weeks after

injection [20]. In order to establish the tumor xenotransplantation model, HNC xenograft tumor was injected into nude mice. FaDu/shNC and FaDu/shAhrr cells (2×10^6 cells) were injected into four weeks male BALB/c nude mice subcutaneously (LAE Biotech), and each group included 20 mice. The experimental animals were grouped according to the randomization formula. Researchers were not aware of the group allocation at the different stages of the experiment during the allocation, the conduct of the experiment, the outcome assessment, and the data analysis. All animal experiments were approved by the Ethics Committee of the medical school of Shanghai Jiaotong University.

Western blot and quantitative analysis

As previously mentioned, Western blot analysis was performed using an antibody against AHRR, EPAS1, HIF-1β, caspase-3, VEGFD, and GAPDH (Shanghai, Beyotime). GAPDH is used as internal parameter control.

Human Lymphatic Endothelial Cells (HLEC) migration analysis

According to the manufacturer's instructions, HLEC migration tests were performed using Falcon™ [21]. Then, 600 μL of tumor supernatant was added to the lower chamber, and 300 μL of serum-free medium containing 1×10^4 HLECs was added to the Transwell chamber and incubated with 5% CO_2 at 37°C for one day. As mentioned earlier, cells were incubated with subsequent tumor procedures.

Endothelial tube formation assay

The HLECs were cultured in tumor supernatant on 96-well plate at a density of 1×10^3 cells/well for eight hours. The plate was precoated at 37°C for three hours with 50 μL Matrigel (BD Bioscience). After 8 hours of culture, tubular image was collected and analyzed by Image PP software. Assessment of each case in triplicate.

Histomorphological assay of lymphangiogenesis

As mentioned earlier, lymphangiogenesis was assessed by vascular density using anti-LYVE-1 antibody. In short, the area with the highest vessel density in the tumor area was photographed, and the digital image of LYVE-1 positive lymphatic vessels was photographed. Then, percentage of the total tissue area was analyzed by Image software.

RNA extraction and RT q-PCR detection

According to the manufacturer's illustration, total RNA was extracted from the samples using Trizol reagent (California, Invitrogen, USA) [22]. Primers for VEGFD used reverse (5'-GGGAACGCTCCAGGACTTAT-3') and forward (5'-GAGGGCAGAATCATCACGAA-3'). This ΔΔCt value is obtained from each sample by subtracting ΔCt of the reference sample was extracted from ΔCt. Fold changes were identified as $2^{-\Delta\Delta Ct}$.

Luciferase report analysis

According to the manufacturer's instructions, luciferase activity was checked using double luciferase analysis (Manassas, VA). The AHRR promoter fragment was cloned into pGL3 vector and amplified from human genomic DNA.

Statistical analysis

Statistical significance of the difference was evaluated with the unpaired t-test for comparisons between 2 means and with one-way analysis of variance. The data set was analyzed by one-way analysis of variance, and the distribution of cell survival data was preliminarily verified by K-S test. The tumor volume of mice was measured using GraphPad prism 8.0 (CA, SanDiego, USA). The lowest significant level was $P<0.05$.

Results

Expression of VEGFD and lymphangiogenesis in tissue section of $Ahrr^{low}$ and $Ahrr^{high}$ HNC

As shown in **Figure 1A**, HNC tissues section showed different degrees of immunoreactive score (IRS). In HNC tissues, the expression of VEGFD was correlated with AHRR level (**Figure 1B**). Overall, these results clearly indicated that the expression of AHRR had an obvious positive correlation with VEGFD expression (**Figure 1C**). Hypoxia has been shown to regulate the production of VEGFD in HNC. Then we next determine how the induction was stimulated by the AHRR. The latter was indicated as lymphat-

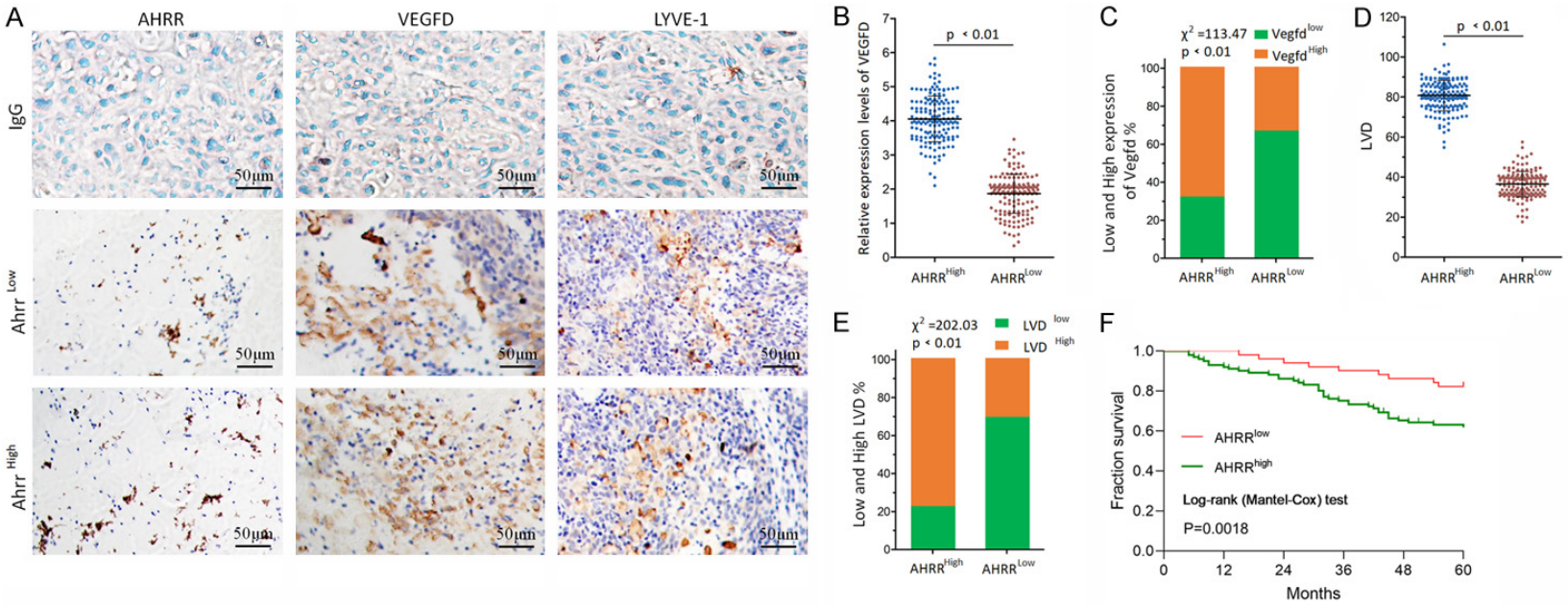

Figure 1. The expression of VEGFD and lymphangiogenesis in *Ahrr*^{low} and *Ahrr*^{high} HNC. A. The immunohistochemical images of low and high expression in HNC were analyzed with unrelated IgG as negative control. B. VEGFD concentrations were measured by enzyme immunoassay in HNC tissues. The mean VEGFD concentration was used to calculate the mean VEGFD concentration for *Ahrr*^{low} and *Ahrr*^{high} HNC. C. Having shown that VEGFD production in the HNC can be stimulated by hypoxia exposure, we next determined how induction was regulated by the AHRR. D, E. LVD scores and percentage of high or low AHRR expression in tumors. Horizontal lines represent the median. F. Comparison of cumulative five-year survival curves of patients with HNC according to independent AHRR expression-related factors with the Log-rank method. The postoperative survival rate of patients with high expression levels of AHRR was poorer than those with lower expression of AHRR. The scale bar represents 50 μm (P<0.01).

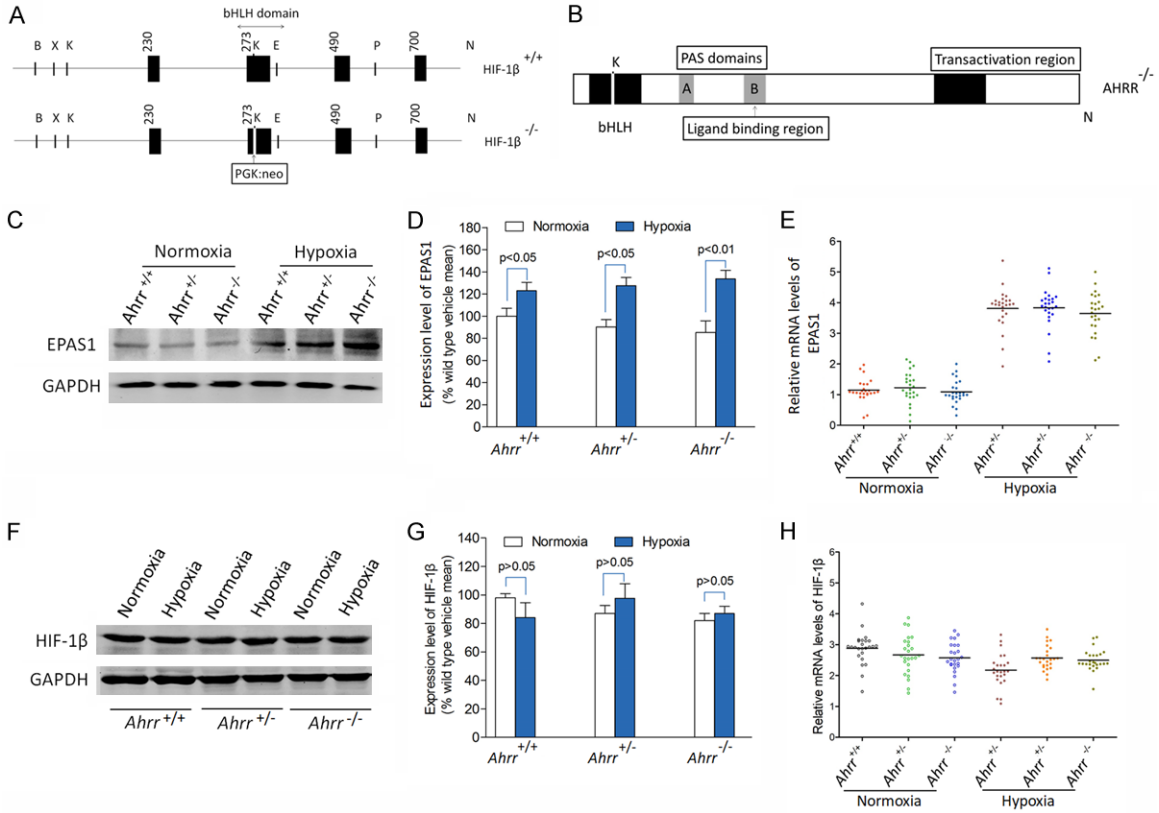

Figure 2. EPAS1 and HIF-1β protein levels in *Ahrr*$^{+/+}$, *Ahrr*$^{+/-}$ and *Ahrr*$^{-/-}$ FaDu cell cultures. A, B. HIF-1β is a member of class II bHLH/PAS protein family, a common binding partner of EPAS1 and AHRR, and an important basis for the interaction between the two signaling pathways. C-E. EPAS1 protein levels were determined by enzyme immunoassay on 10 μg total protein isolated from FaDu cell cultured with normoxia or hypoxia. F-H. HIF-1β protein levels were determined by western blot analysis of 10 μg total protein isolated from FaDu cell cultured with normoxia or hypoxia. Band density was calculated for each protein and expressed relative to GAPDH band density. Data are mean ± SD in triplicates in an independent experiment, which was repeated at least for three times with the same results (P<0.01).

ic vessel density (LVD), and they were analyzed in our HNC sample cohort to correlate with AHRR (**Figure 1D**, **1E**). Log-rank analysis revealed a significant association between high expression of AHRR in cancerous tissue and a worse prognosis (P=0.0018) (**Figure 1F**).

AHRR competes with EPAS1 to combine HIF-1β in cultured Ahrr$^{+/+}$*, Ahrr*$^{+/-}$ *and Ahrr*$^{-/-}$ *HNC*

HIF-1β, the co-binding partner of EPAS1 and AHRR, is a member of the class II bHLH/PAS protein family and an important basis for the interaction between the two signal pathways (**Figure 2A**, **2B**). Although Akt phosphorylation activated PI3K Signal is similar in *Ahrr*$^{+/+}$, *Ahrr*$^{+/-}$ and *Ahrr*$^{-/-}$ FaDu cells, it is uncertain whether more VEGFD activity in *Ahrr*$^{-/-}$ FaDu cells can be attributed to the increase of downstream protein levels (**Figure 2C**, **2D**). This can be interpreted by the elevated levels of background proteins of EPAS1 or HIF-1β, or by the increased sensitivity of these proteins to hypoxia-induced hypoxia in *Ahrr*$^{-/-}$ FaDu cells. The levels of EPAS1 protein in *Ahrr*$^{+/+}$, *Ahrr*$^{+/-}$ and *Ahrr*$^{-/-}$ mice exposed to vehicle or hypoxia were significantly different by enzyme-linked immunosorbent assay (**Figure 2E**). Western blot analysis showed that HIF-1β protein level was not associated with hypoxic exposure and AHRR genotype (**Figure 2F-H**).

Hypoxic activation of the EPAS1/PI3K/VEGFD signaling axis in Ahrr$^{+/+}$*, Ahrr*$^{+/-}$ *and Ahrr*$^{-/-}$ *HNC*

Although hypoxia-induced VEGFD expression in *Ahrr*$^{+/+}$ FaDu HNC is more obvious than that in *Ahrr*$^{-/-}$ and *Ahrr*$^{+/-}$ FaDu HNC, it is necessary to

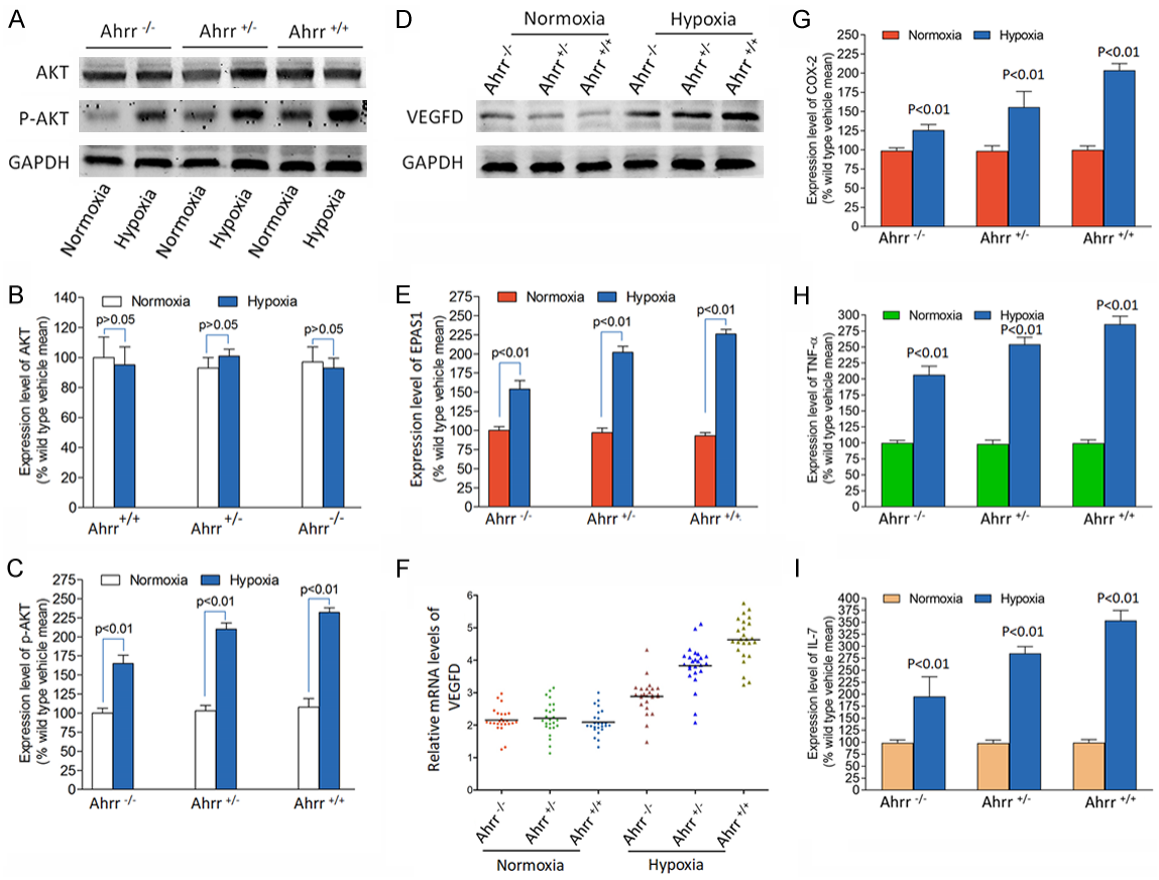

Figure 3. Hypoxia activation of the EPAS1/PI3K/VEGFD signaling axis in *Ahrr*$^{+/+}$, *Ahrr*$^{+/-}$ and *Ahrr*$^{-/-}$ FaDu HNC. Western blot determination of Akt (A, B) and p-Akt (C) and VEGFD (D-F) protein band density was determined using 10 μg total protein isolated from HNC cultured with vehicle or hypoxia (n=15 for each group and each *Ahrr* genotype). (B, C) There was no significant difference in the level of total Akt protein in the medium exposed to *Ahrr*$^{+/+}$, *Ahrr*$^{+/-}$ and *Ahrr*$^{-/-}$ FaDu HNC, nor was there any difference with any *Ahrr* genotype exposed to hypoxia. (D) The increased sensitivity of *Ahrr*$^{+/+}$ FaDu HNC to VEGFD under hypoxia cannot be explained by the increased expression of Akt protein. (E, F) These results suggest that the greater sensitivity to stimulating VEGFD production in *Ahrr*$^{+/+}$ FaDu HNC occurs at a point downstream of Akt activation. (G-I) Under hypoxia, tumor cells release more inflammatory factors. Band density was calculated for each protein and expressed relative to band density of GAPDH (P<0.01).

understand whether hypoxia-induced PI3K signal exists in all AHRR genotypes of HNC. In order to quantitatively stimulate PI3K signaling upstream of EPAS1 by hypoxia, we used Western blot to detect Akt protein phosphorylation (**Figure 3A**). There was no significant difference in total Akt protein level in the medium exposed to *Ahrr*$^{+/+}$, *Ahrr*$^{+/-}$ and *Ahrr*$^{-/-}$ FaDu HNC, nor was there any difference with any AHRR genotype exposed to hypoxia (**Figure 3B**). However, compared with cells exposed to vectors, the activation of PI3K signals in all *Ahrr*$^{+/+}$, *Ahrr*$^{+/-}$ and *Ahrr*$^{-/-}$ FaDu HNC exposed to hypoxia increased by phosphorylation of Akt (**Figure 3C**). In the presence of a single vector, the phosphorylated Akt band density of each AHRR genotype HNC was similar, and the induction amount of each AHRR genotype HNC was similar after hypoxia. Therefore, the higher sensitivity of *Ahrr*$^{-/-}$ HNC to VEGFD under hypoxia cannot be explained by the increased expression of Akt protein (**Figure 3D**). These findings indicate that greater sensitivity to stimulating VEGFD production in *Ahrr*$^{+/+}$ HNC occurs downstream of Akt activation (**Figure 3E**, **3F**). Under hypoxia, tumor cells release more inflammatory factors (**Figure 3G-I**).

Interaction of AHRR, EPAS1, and ARNT in HNC cells of AHRR-null or wild-type

Quantitative RT-PCR analysis showed that the amounts of EPAS1 and ARNT mRNAs were

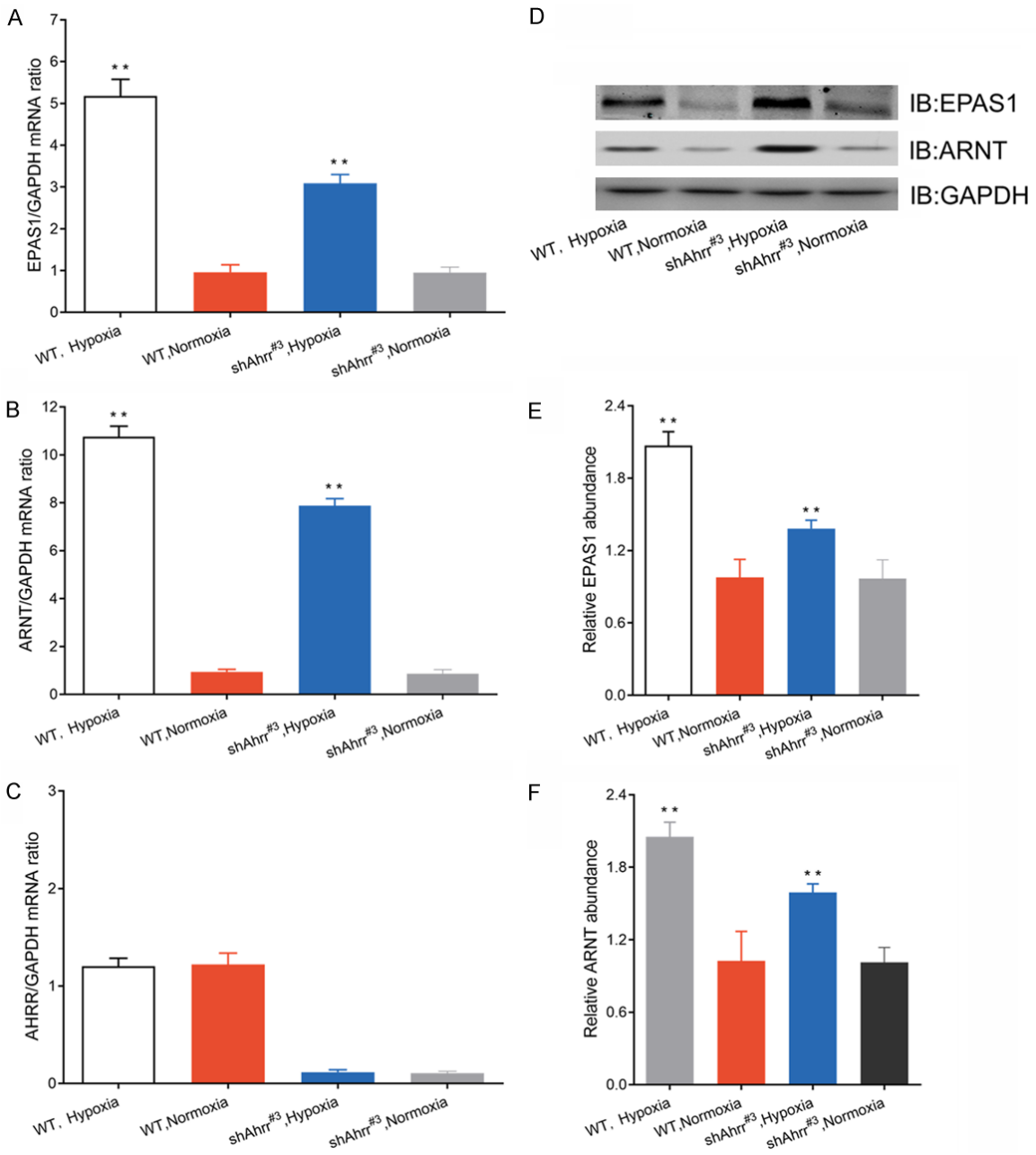

Figure 4. Interaction of EPAS1, ARNT, and AHRR in HNC cells of AHRR-null or wild-type. A-C. Quantitative RT-PCR analysis of EPAS1, ARNT, and AHRR mRNAs in HNC cells 2 days after hypoxia. The data were standardized by the abundance of GAPDH mRNA. D-F. Western blotting analysis (IB) of EPAS1, ARNT and GAPDH in nuclear extracts of isolated HNC cells after 3 days of hypoxia. All quantitative data were mean ± SEM of HNC cells in each group. **P<0.05 versus HNCs and HNCs/shNT.

increased in HNC cells of both AHRR-null and wild-type at 2 days after hypoxia (**Figure 4A**, **4B**). The amount of AHRR mRNA in HNC cells did not differ in wild-type cells at 3 days after hypoxia (**Figure 4C**). These increases were significantly lower in AHRR-null cells than in wild-type cells. Immunoblot analysis also revealed similar changes in the nuclear abundance of EPAS1 and ARNT proteins at 3 days after hypoxia (**Figure 4D-F**).

Effect of shRNA silencing AHRR on lymphangiogenesis in HNCs

In order to detect the regulatory effect of AHRR on lymphangiogenesis in HNC cells, an *in vitro*

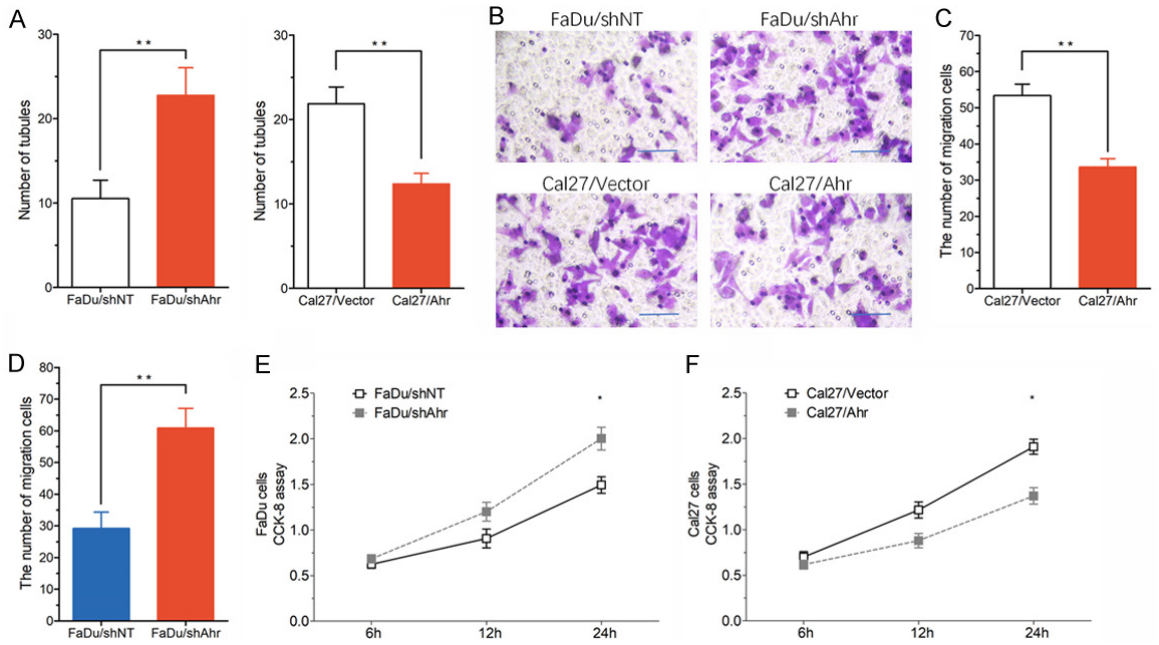

Figure 5. Effects of *Ahrr* knockdown on lymphangiogenesis in HNC tumors. A. Effect of conditioned medium (CM) from indicated HNC sublines on HLECs tubule formation. B-D. Effect of CM from indicated HNC sublines on HLECs transwell migration. E, F. Effect of CM from indicated HNC sublines on HLECs proliferation, measured by CCK-8. **P<0.05 versus HNCs and HNCs/shNT.

endothelial tubule formation test was used. Conditioned medium (CM) refers to the culture medium after removing cells. In the experiment, the cells were removed by high-speed centrifugation from cell culture medium. CM was collected from Ahrr-modified HNC subline and added to 3D culture HLECs. Compared with CM of FaDu/shAhrr cells, the formation of tubules by HLECs induced by FaDu/shNT cells was significantly enhanced, while the formation of tubules by HLECs induced by CM of Cal27/Vector cells was significantly less than that of Cal27/Ahrr cells (**Figure 5A**). Tumor cell CM may regulate the formation of HLECs tubules by altering endothelial cell proliferation or migration. We studied these two possibilities by Transwell and CCK-8 assay, and found that Ahrr-high CM promoted the migration (**Figure 5B-D**) and viability of HLECs (**Figure 5E**, **5F**).

Effects of Ahrr knockdown and EPAS1/VEGFD signal axis on LNM in HNC tumors in vivo

To explore the role of AHRR in lymphangiogenesis and LNM *in vivo*, shAhrr and shNT cells were inoculated into mice. Immunohistochemical detection of tumors in mice showed that lymphangiogenesis of *Ahrr*$^{+/+}$ tumors was higher than that of *Ahrr*$^{-/-}$ and *Ahrr*$^{+/-}$ tumors (**Figure 6A**). In addition, the LNM of shNT tumors was significantly higher than that of shAhrr$^{\#3}$ tumors (**Figure 6B**, **6C**).

Discussion

LNM accounts for more than 90% of the total mortality of solid tumors [1]. In current studies, we found that before tumorigenesis, AHRR can increase the production of VEGFD in transplanted tumors, which is a key role of lymphangiogenesis and tumor growth [23-25]. In conclusion, these findings indicate that the increased expression of AHRR in HNC cells up-regulates the expression of Akt phosphorylation and VEGFD, thus promoting lymphangiogenesis and LNM in HNC cells.

In the study, we found the inhibition of Akt phosphorylation by Ahrr gene knock-out decreased lymphangiogenesis, LNM and VEGFD expression. The hypoxic conditions of precancerous epithelial cells during accelerated growth stabilized or up-regulated EPAS1, which promoted the local production of lymphangiogenesis factors [26]. These studies are in accordance with PI3K activation of VEGFD, but

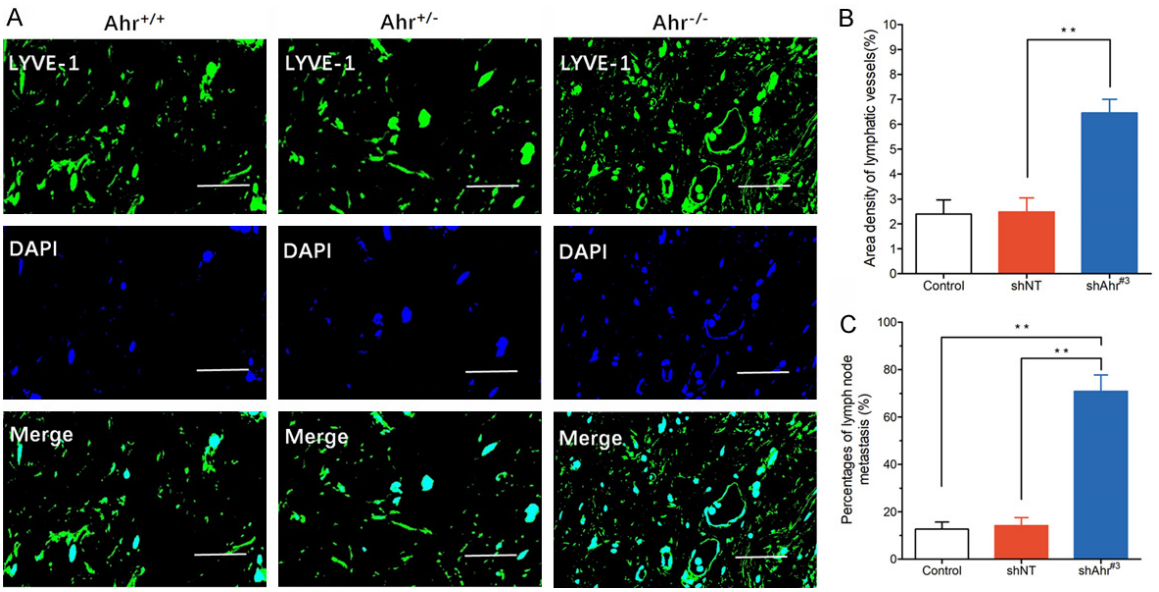

Figure 6. Effects of *Ahrr* knockdown and EPAS1/VEGFD signal axis on LNM in HNC tumors in vivo. A. Transplanted tumor of *Ahrr*$^{-/-}$, *Ahrr*$^{+/+}$ and *Ahrr*$^{+/-}$ HNCs were harvested as described in Materials and Methods. Frozen sections of shNT and shAhrr$^{\#3}$ tumors were stained for lymphatic vessels with anti-LYVE-1 antibody (green), followed by staining with DAPI (blue). Scale bar 100 μm. B, C. Quantification of lymphatic vessels in shNT and shAhrr$^{\#3}$ transplanted tumors. Data were expressed as mean area density of LYVE-1-positive pixels per microscopic field (mean ± SD). **P<0.05 versus shNT. Frequency of LNM in HNCs (n=20), and shNT (n=19) and shAhrr$^{\#3}$ (n=17) tumor-bearing mice.

also indicate that EPAS1 expression level is upregulated in HNCs [27]. These studies suggest that AHRR enhances the sensitivity of HNC to VEGFD signal pathways. In addition, the loss of tensin homologues and phosphatase is common in HNC carcinogenesis to avoid the inhibition of PI3K signal [28]. Therefore, AHRR regulates the production of VEGFD through its interaction with HIF-1β, which may induce the cascade of multiple signals in the carcinogenesis of HNC [29]. Similarly, the existence of AHRR in many tissues does not exclude the possibility of the activation of EPAS1, which may also be induced by the interaction between AHRR and HIF-1β in many other human cancers dependent on lymphangiogenesis [30].

According to our findings, we believe that AHRR regulates the production of VEGFD by enhancing HIF-1β, thus accelerating the interaction with stable EPAS1. When diffuse epithelial hyperplasia was observed in all HNCs, AHRR interacted with HIF-1β, enhancing the expression of EPAS1 to stably stimulate VEGFD production, resulting in an increase in tumor growth [31, 32]. When AHRR is induced, the unimpeded interaction between EPAS1/HIF-1β increases the production of VEGFD, leading to a more universal tumorigenesis [33]. The interaction of AHRR-HIF-1β may activate the production of VEGFD and the growth of tumors in oxygen-deficient environment induced by the excessive proliferation of HNC or the increase of growth factors previously associated with HNC carcinogenesis [16]. This effect does not decrease the activation of PI3K cascade reaction, but it decreases the physiological response of EPAS1 to the activation of downstream VEGFD production and subsequent growth of tumors.

Conclusions

Selective AHRR regulators have been shown to promote the proliferation of HNC in the absence of AHRR-mediated toxicity correlated with dioxin exposure. These studies indicate that stimulating AHRR signal can increase the carcinogenesis of HNC *in vivo* by interacting with HIF-1β. Potential AHRR regulators enhancing HNC tumors are currently being explored.

Acknowledgements

We thank the laboratory team for its collaboration. This study was funded by grants from the Pudong New Area health system discipline

leader project (No. PWRd2021-04); Shanghai Pudong Science & Technology Development Foundation (No. PKJ2021-Y13); Key Disciplines Group Construction Project of Pudong Health Bureau of Shanghai (No. PWZxq2017-04 and No. 2022GPY-A05); Key sub specialty construction project of Pudong Health Bureau of Shanghai (No. PWZy2020-06); Research Grant for Health Science and Technology of Pudong Health Bureau of Shanghai (No. PW2019D-4) and Key Specialist Construction Project of Health Bureau of Shanghai (No. ZK2019C06).

Disclosure of conflict of interest

None.

Address correspondence to: An Hu, Gongli Hospital, Second Military Medical University, Pudong New Area, 219 Miaopu Road, Shanghai 200135, China. Tel: +86-13764147286; E-mail: juanitohuan@163.com

References

[1] de Bono JS, Concin N, Hong DS, Thistlethwaite FC, Machiels JP, Arkenau HT, Plummer R, Jones RH, Nielsen D, Windfeld K, Ghatta S, Slomovitz BM, Spicer JF, Yachnin J, Ang JE, Mau-Sorensen PM, Forster MD, Collins D, Dean E, Rangwala RA and Lassen U. Tisotumab vedotin in patients with advanced or metastatic solid tumours (InnovaTV 201): a first-in-human, multicentre, phase 1-2 trial. Lancet Oncol 2019; 20: 383-393.

[2] Cohen EEW, Soulieres D, Le Tourneau C, Dinis J, Licitra L, Ahn MJ, Soria A, Machiels JP, Mach N, Mehra R, Burtness B, Zhang P, Cheng J, Swaby RF and Harrington KJ; KEYNOTE-040 investigators. Pembrolizumab versus methotrexate, docetaxel, or cetuximab for recurrent or metastatic head-and-neck squamous cell carcinoma (KEYNOTE-040): a randomised, open-label, phase 3 study. Lancet 2019; 393: 156-167.

[3] Haddad RI, Massarelli E, Lee JJ, Lin HY, Hutcheson K, Lewis J, Garden AS, Blumenschein GR, William WN, Pharaon RR, Tishler RB, Glisson BS, Pickering C, Gold KA, Johnson FM, Rabinowits G, Ginsberg LE, Williams MD, Myers J, Kies MS and Papadimitrakopoulou V. Weekly paclitaxel, carboplatin, cetuximab, and cetuximab, docetaxel, cisplatin, and fluorouracil, followed by local therapy in previously untreated, locally advanced head and neck squamous cell carcinoma. Ann Oncol 2019; 30: 471-477.

[4] Lee JW, Parameswaran J, Sandoval-Schaefer T, Eoh KJ, Yang DH, Zhu F, Mehra R, Sharma R, Gaffney SG, Perry EB, Townsend JP, Serebriiskii IG, Golemis EA, Issaeva N, Yarbrough WG, Koo JS and Burtness B. Combined aurora kinase A (AURKA) and WEE1 inhibition demonstrates synergistic antitumor effect in squamous cell carcinoma of the head and neck. Clin Cancer Res 2019; 25: 3430-3442.

[5] Puram SV, Tirosh I, Parikh AS, Patel AP, Yizhak K, Gillespie S, Rodman C, Luo CL, Mroz EA, Emerick KS, Deschler DG, Varvares MA, Mylvaganam R, Rozenblatt-Rosen O, Rocco JW, Faquin WC, Lin DT, Regev A and Bernstein BE. Single-cell transcriptomic analysis of primary and metastatic tumor ecosystems in head and neck cancer. Cell 2017; 171: 1611-1624, e1624.

[6] Carnielli CM, Macedo CCS, De Rossi T, Granato DC, Rivera C, Domingues RR, Pauletti BA, Yokoo S, Heberle H, Busso-Lopes AF, Cervigne NK, Sawazaki-Calone I, Meirelles GV, Marchi FA, Telles GP, Minghim R, Ribeiro ACP, Brandao TB, de Castro G Jr, Gonzalez-Arriagada WA, Gomes A, Penteado F, Santos-Silva AR, Lopes MA, Rodrigues PC, Sundquist E, Salo T, da Silva SD, Alaoui-Jamali MA, Graner E, Fox JW, Coletta RD and Paes Leme AF. Combining discovery and targeted proteomics reveals a prognostic signature in oral cancer. Nat Commun 2018; 9: 3598.

[7] Sennino B, Ishiguro-Oonuma T, Schriver BJ, Christensen JG and McDonald DM. Inhibition of c-Met reduces lymphatic metastasis in RIP-Tag2 transgenic mice. Cancer Res 2013; 73: 3692-3703.

[8] Dufies M, Giuliano S, Ambrosetti D, Claren A, Ndiaye PD, Mastri M, Moghrabi W, Cooley LS, Ettaiche M, Chamorey E, Parola J, Vial V, Lupu-Plesu M, Bernhard JC, Ravaud A, Borchiellini D, Ferrero JM, Bikfalvi A, Ebos JM, Khabar KS, Grépin R and Pagès G. Sunitinib stimulates expression of VEGFC by tumor cells and promotes lymphangiogenesis in clear cell renal cell carcinomas. Cancer Res 2017; 77: 1212-1226.

[9] Wang CA, Jedlicka P, Patrick AN, Micalizzi DS, Lemmer KC, Deitsch E, Casas-Selves M, Harrell JC and Ford HL. SIX1 induces lymphangiogenesis and metastasis via upregulation of VEGF-C in mouse models of breast cancer. J Clin Invest 2012; 122: 1895-1906.

[10] Der Vartanian A, Quetin M, Michineau S, Aurade F, Hayashi S, Dubois C, Rocancourt D, Drayton-Libotte B, Szegedi A, Buckingham M, Conway SJ, Gervais M and Relaix F. PAX3 confers functional heterogeneity in skeletal muscle stem cell responses to environmental stress. Cell Stem Cell 2019; 24: 958-973, e9.

[11] Zajda K, Rak A, Ptak A and Gregoraszczuk EL. Compounds of PAH mixtures dependent interaction between multiple signaling pathways in granulosa tumour cells. Toxicol Lett 2019; 310: 14-22.
[12] Stegen S, Laperre K, Eelen G, Rinaldi G, Fraisl P, Torrekens S, Van Looveren R, Loopmans S, Bultynck G, Vinckier S, Meersman F, Maxwell PH, Rai J, Weis M, Eyre DR, Ghesquiere B, Fendt SM, Carmeliet P and Carmeliet G. HIF-1alpha metabolically controls collagen synthesis and modification in chondrocytes. Nature 2019; 565: 511-515.
[13] Hsu SL, Yin TC, Shao PL, Chen KH, Wu RW, Chen CC, Lin PY, Chung SY, Sheu JJ, Sung PH, Chen CY, Wang CJ, Yip HK and Lee MS. Hyperbaric oxygen facilitates the effect of endothelial progenitor cell therapy on improving outcome of rat critical limb ischemia. Am J Transl Res 2019; 11: 1948-1964.
[14] Chen Y, Zhao B, Zhu Y, Zhao H and Ma C. HIF-1-VEGF-Notch mediates angiogenesis in temporomandibular joint osteoarthritis. Am J Transl Res 2019; 11: 2969-2982.
[15] Oziolor EM, Reid NM, Yair S, Lee KM, Guberman VerPloeg S, Bruns PC, Shaw JR, Whitehead A and Matson CW. Adaptive introgression enables evolutionary rescue from extreme environmental pollution. Science 2019; 364: 455-457.
[16] Rothhammer V and Quintana FJ. The aryl hydrocarbon receptor: an environmental sensor integrating immune responses in health and disease. Nat Rev Immunol 2019; 19: 184-197.
[17] Cui H, Gu X, Chen J, Xie Y, Ke S, Wu J, Golovko A, Morpurgo B, Yan C, Phillips TD, Xie W, Luo J, Zhou Z and Tian Y. Pregnane X receptor regulates the AhR/Cyp1A1 pathway and protects liver cells from benzo-[alpha]-pyrene-induced DNA damage. Toxicol Lett 2017; 275: 67-76.
[18] Huang JJ, Shi YQ, Li RL, Hu A, Lu ZY, Weng L, Han YP, Wang SQ, Zhang L, Hao CN and Duan JL. Therapeutic ultrasound protects HUVECs from ischemia/hypoxia-induced apoptosis via the PI3K-Akt pathway. Am J Transl Res 2017; 9: 1990-1999.
[19] Hu A, Huang JJ, Zhang JF, Dai WJ, Li RL, Lu ZY, Duan JL, Li JP, Chen XP, Fan JP, Xu WH and Zheng HL. Curcumin induces G2/M cell cycle arrest and apoptosis of head and neck squamous cell carcinoma in vitro and in vivo through ATM/Chk2/p53-dependent pathway. Oncotarget 2017; 8: 50747-50760.
[20] Tang X, Sun Y, Wan G, Sun J and Pan C. Knockdown of YAP inhibits growth in Hep-2 laryngeal cancer cells via epithelial-mesenchymal transition and the Wnt/β-catenin pathway. BMC Cancer 2019; 19: 654.
[21] Petersen CH, Mahmood B, Badsted C, Dahlby T, Rasmussen HB, Hansen MB and Bindslev N. Possible predisposition for colorectal carcinogenesis due to altered gene expressions in normal appearing mucosa from patients with colorectal neoplasia. BMC Cancer 2019; 19: 643.
[22] Wang W, Li Y, Liu N, Gao Y and Li L. MiR-23b controls ALDH1A1 expression in cervical cancer stem cells. BMC Cancer 2017; 17: 292.
[23] Kubli SP, Bassi C, Roux C, Wakeham A, Gobl C, Zhou W, Jafari SM, Snow B, Jones L, Palomero L, Thu KL, Cassetta L, Soong D, Berger T, Ramachandran P, Baniasadi SP, Duncan G, Lindzen M, Yarden Y, Herranz C, Lazaro C, Chu MF, Haight J, Tinto P, Silvester J, Cescon DW, Petit A, Pettersson S, Pollard JW, Mak TW, Pujana MA, Cappello P and Gorrini C. AhR controls redox homeostasis and shapes the tumor microenvironment in BRCA1-associated breast cancer. Proc Natl Acad Sci U S A 2019; 116: 3604-3613.
[24] Shi CS, Kuo KL, Lin WC, Chen MS, Liu SH, Liao SM, Hsu CH, Chang YW, Chang HC and Huang KH. Neddylation inhibitor, MLN4924 suppresses angiogenesis in huvecs and solid cancers: in vitro and in vivo study. Am J Cancer Res 2020; 10: 953-964.
[25] Shigetomi S, Imanishi Y, Shibata K, Sakai N, Sakamoto K, Fujii R, Habu N, Otsuka K, Sato Y, Watanabe Y, Shimoda M, Kameyama K, Ozawa H, Tomita T and Ogawa K. VEGF-C/Flt-4 axis in tumor cells contributes to the progression of oral squamous cell carcinoma via upregulating VEGF-C itself and contactin-1 in an autocrine manner. Am J Cancer Res 2018; 8: 2046-2063.
[26] Kim J, Kim HY, Song SY, Go SH, Sohn HS, Baik S, Soh M, Kim K, Kim D, Kim HC, Lee N, Kim BS and Hyeon T. Synergistic oxygen generation and reactive oxygen species scavenging by manganese ferrite/ceria co-decorated nanoparticles for rheumatoid arthritis treatment. ACS Nano 2019; 13: 3206-3217.
[27] Garmy-Susini B, Avraamides CJ, Desgrosellier JS, Schmid MC, Foubert P, Ellies LG, Lowy AM, Blair SL, Vandenberg SR, Datnow B, Wang HY, Cheresh DA and Varner J. PI3Kalpha activates integrin alpha4beta1 to establish a metastatic niche in lymph nodes. Proc Natl Acad Sci U S A 2013; 110: 9042-9047.
[28] Nakajima T, Anayama T, Koike T, Shingyoji M, Castle L, Kimura H, Yoshino I and Yasufuku K. Endobronchial ultrasound doppler image features correlate with mRNA expression of HIF1-alpha and VEGF-C in patients with non-small-cell lung cancer. J Thorac Oncol 2012; 7: 1661-1667.

[29] Mayer AK, Mahajnah M, Thomas MG, Cohen Y, Habib A, Schulze M, Maconachie GDE, AlMoallem B, De Baere E, Lorenz B, Traboulsi EI, Kohl S, Azem A, Bauer P, Gottlob I, Sharkia R and Wissinger B. Homozygous stop mutation in AHR causes autosomal recessive foveal hypoplasia and infantile nystagmus. Brain 2019; 41: 1528-1534.

[30] Gronke K, Hernandez PP, Zimmermann J, Klose CSN, Kofoed-Branzk M, Guendel F, Witkowski M, Tizian C, Amann L, Schumacher F, Glatt H, Triantafyllopoulou A and Diefenbach A. Interleukin-22 protects intestinal stem cells against genotoxic stress. Nature 2019; 566: 249-253.

[31] Gerard D, Schmidt F, Ginolhac A, Schmitz M, Halder R, Ebert P, Schulz MH, Sauter T and Sinkkonen L. Temporal enhancer profiling of parallel lineages identifies AHR and GLIS1 as regulators of mesenchymal multipotency. Nucleic Acids Res 2019; 47: 1141-1163.

[32] Hamano H, Niimura T, Horinouchi Y, Zamami Y, Takechi K, Goda M, Imanishi M, Chuma M, Izawa-Ishizawa Y, Miyamoto L, Fukushima K, Fujino H, Tsuchiya K, Ishizawa K, Tamaki T and Ikeda Y. Proton pump inhibitors block iron absorption through direct regulation of hepcidin via the aryl hydrocarbon receptor-mediated pathway. Toxicol Lett 2020; 318: 86-91.

[33] Singh R, Chandrashekharappa S, Bodduluri SR, Baby BV, Hegde B, Kotla NG, Hiwale AA, Saiyed T, Patel P, Vijay-Kumar M, Langille MGI, Douglas GM, Cheng X, Rouchka EC, Waigel SJ, Dryden GW, Alatassi H, Zhang HG, Haribabu B, Vemula PK and Jala VR. Enhancement of the gut barrier integrity by a microbial metabolite through the Nrf2 pathway. Nat Commun 2019; 10: 89.